AIAA JOURNAL
Vol. 53, No. 9, September 2015

Experimental Investigation of the Starting Behavior of a Three-Dimensional Scramjet Intake

Andreas K. Flock* and Ali Gülhan†
DLR, German Aerospace Center, 51147 Cologne, Germany

DOI: 10.2514/1.J053786

To this date, there is no generally valid method to accurately predict intake starting for a certain three-dimensional scramjet intake configuration. Therefore, experiments are conducted at Mach 6 and 7 in a blowdown wind tunnel on a three-dimensional intake model, equipped with a movable cowl and therefore variable internal contraction. The internal contraction is slowly decreased, and the performance parameters at the interface to the combustion chamber are measured with a rake. The general trends from the Kantrowitz diagram were able to be reproduced, namely enhanced intake starting for higher freestream Mach numbers and lower internal contraction ratios. Furthermore, the effect of the angle of attack was twofold: When the intake was pitched, the leading-edge shock decreased in strength, and the intake showed improved starting characteristics. For increasing yaw angles, intake starting was hindered. Exchanging the *V*-shaped cowl with a straight-cowl geometry improved intake starting due to the additional mass spillage. Once the intake was started, increasing the internal contraction ratio to 2.56 did not cause the intake to unstart for all Mach numbers investigated.

Nomenclature

A	=	cross-sectional area, m^2
CR	=	contraction ratio
M	=	Mach number
$\dot{m}$	=	mass flow rate, kg/s
n	=	number of data points
p	=	pressure, N/m^2
q	=	dynamic pressure, N/m^2
Re	=	Reynolds number
s	=	straight
T	=	temperature, K
v	=	velocity, m/s
V	=	V-shaped
x, y, z	=	local coordinates, m
α, β	=	pitch and yaw angle, deg
γ	=	ratio of specific heats for air
Π	=	pressure ratio
ρ	=	density, kg/m^3
ϕ	=	sample variable

Subscripts

cl	=	cowl closure
j	=	index variable
i	=	internal portion
o	=	overall configuration
pit	=	pitot
st	=	static
t	=	total condition
th	=	throat
tot	=	total
w	=	wall
∞	=	freestream condition

Presented as Paper 2014-2934 at the 19th AIAA International Space Planes and Hypersonic Systems and Technologies Conference, Atlanta, GA, 16–20 June 2014; received 21 July 2014; revision received 28 November 2014; accepted for publication 4 December 2014; published online 26 February 2015.

*Ph.D. Candidate, Supersonic and Hypersonic Technology Department, Institute of Aerodynamics and Flow Technology, Linder Höhe; andreas.flock@dlr.de. Student Member AIAA (Corresponding Author).

†Head, Supersonic and Hypersonic Technology Department, Institute of Aerodynamics and Flow Technology, Linder Höhe.

I. Introduction

THE supersonic combustion ramjet engine is a key propulsion technology when exceeding a Mach number of approximately 5. In any kind of air-breathing supersonic engine, the intake design is crucial for its performance, and in the scramjet engine, the intake serves as the only compression system in the engine cycle [1]. Therefore, a proper understanding of the flow phenomena within the intake and its performance is vital for successful operation of the overall engine system.

The focus in the current paper is on the scramjet intake starting behavior. The exit flow of the intake or of a supersonic diffuser in general can either be subsonic or supersonic [2], with the latter being the case desired and being referred to as started intake flow hereafter. Subsonic flow through the intake can lead to a severe reduction in mass flow and in overall engine performance or even loss of the vehicle.

A one-dimensional model for starting of supersonic diffusers was proposed by Oswatitsch [3] and Kantrowitz and Donaldson [4]. Despite the fact that Oswatitsch published his results earlier, we have the impression that Kantrowitz's name is more widely associated with the theory, and therefore we will also refer to the Kantrowitz criterion hereafter. It states that a normal shock in front of the intake can be swallowed as long as the flow behind the shock is accelerated right to $M = 1$ at the intake throat. Any further contraction would lead to a detachment of the normal shock from the intake and an intake unstart. The relation between capture area A_∞, cross-sectional area at the throat A_{th}, and freestream Mach number M_∞ can be described by a one-dimensional flow analysis and is given via

$$\frac{A_{th}}{A_\infty} = \left[\frac{\gamma-1}{\gamma+1} + \frac{2}{(\gamma+1)M_\infty^2}\right]^{0.5}\left[\frac{2\gamma}{\gamma+1} - \frac{\gamma-1}{(\gamma+1)M_\infty^2}\right]^{1/(\gamma-1)} \quad (1)$$

where γ is the ratio of specific heats for air. Furthermore, an isentropic limit can be defined from a quasi-one-dimensional analysis for nozzle flow [5], until which an intake is theoretically able to work once it was successfully started:

$$\frac{A_\infty}{A_{th}} = \frac{1}{M_\infty}\left[\frac{2}{\gamma+1}\left(1 + \frac{\gamma-1}{2}M_\infty^2\right)\right]^{(\gamma+1)/(2(\gamma-1))} \quad (2)$$

The previous Kantrowitz criterion and the isentropic limit can be directly applied to fully enclosed intake geometries [4,6,7] but were

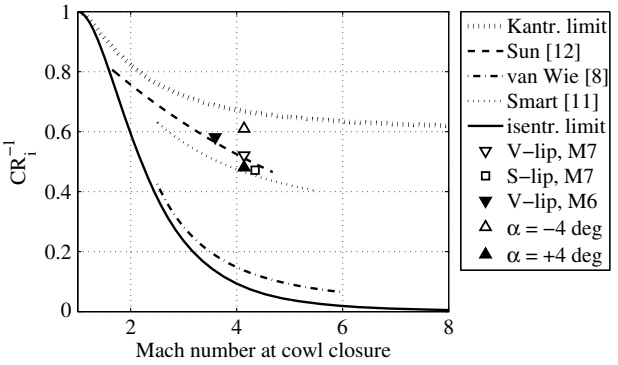

Fig. 1 Kantrowitz criterion [Eq. (1)], along with empirical relations and the isentropic limit [Eq. (2)]; furthermore, the starting internal contraction ratios for the currently investigated intake are shown.

also adopted to partially enclosed intakes [8–10]. Hereafter, A_∞ and M_∞ are replaced by the cross-sectional area A_{cl} and Mach number M_{cl} at the beginning of the fully enclosed part of the intake. Please note that a fully enclosed intake consists of an internal part only, whereas a partially enclosed intake also has an external part. Herein, area ratios are referred to as contraction ratios (CRs), where

$$\mathrm{CR}_o = \frac{A_\infty}{A_{\mathrm{th}}} \tag{3}$$

is the overall contraction ratio, and

$$\mathrm{CR}_i = \frac{A_{\mathrm{cl}}}{A_{\mathrm{th}}} \tag{4}$$

is the internal contraction ratio.

The Kantrowitz criterion and the isentropic limit are displayed in Fig. 1, along with empirical relations, which will be explained subsequently. The region above the Kantrowitz line (dotted) describes a configuration where the intake starts spontaneously, according to the Kantrowitz theory. The area, which is spanned by the Kantrowitz line and the isentropic limit (solid), is the region where an intake does not start spontaneously, according to Kantrowitz, but where an intake could work successfully, once it was properly started. Every intake configuration with an internal contraction ratio exceeding the isentropic limit is never able to work successfully.

In Eq. (1a), quasi-one-dimensional flow was assumed. However, for three-dimensional intake geometries, this assumption is not exact, and intake starting can occur at internal contraction ratios higher than those predicted by Kantrowitz theory. The dotted line in Fig. 1 should therefore be considered as a conservative boundary to determine the intake starting contraction ratio.

Various authors published research on the intake starting process, and selected topics will be captured in the following paragraphs. Sun and Zhang proposed a linear, empirical relation [11] between the area ratio and M_{cl}. Thereto different self-starting intakes taken from experiments found in the literature were plotted in the Kantrowitz diagram and then linearly approximated (see dashed line in Fig. 1). Similarly, Smart [12] proposed a quadratic fit to data of various three-dimensional intakes, and results are valid for $2.5 < M_{\mathrm{cl}} < 5.5$ (Fig. 1).

van Wie et al. investigated intake starting behavior with a generic two-dimensional model of an internal intake [8]. They observed hard and soft versions of intake unstart, depending on the specific configuration of their generic model, which had variable geometry and therefore an adjustable internal contraction ratio, but were not able in all cases to discern the causal effects of hard and soft unstarts. From their data, they introduced an empirical limit for the highest contraction ratios possible, similar to the isentropic limit, but taking into account viscous effects and shock losses (see dashed-dotted line in Fig. 1).

Jacobsen et al. [13] investigated the starting behavior of a circular three-dimensional intake that was designed by a streamline tracing algorithm [14,15] applied to an axisymmetric Busemann flow [16] ("sugar scoop" intake). They observed that the internal contraction ratio of the streamline traced intake itself was too high for self-starting at a freestream Mach number of 4. They investigated two means to enhance intake starting: bleed holes and a movable cowl. Based on numerical simulation, both devices helped the intake to start. Experiments were then performed for the configuration with the movable cowl to verify the computational results.

Finally, Mölder et al. [9], Veillard et al. [10], and Timofeev et al. [17] published numerous papers on intake starting. They studied different ways of promoting intake starting, such as overboard spillage, overspeeding, permeable walls, or by employing unsteady effects. A general approach was to first articulate the intake geometry into the region where the intake will self-start and then change the geometry via movable parts toward the isentropic limit. Their paper on intake starting gives a good overview of the different techniques and mechanisms [17].

To establish a better understanding of the starting behavior of supersonic diffusers, we performed experiments with a three-dimensional scramjet intake. In the following, the experimental apparatus and techniques are described. Results of the conducted starting experiments are presented and put into perspective with results from the literature. Finally, the main findings, as well as the physical insights that can be extracted from our results, are highlighted.

II. Experimental Facility and Model

In this section, three topics will be outlined: First, the wind-tunnel facility H2K at DLR, German Aerospace Center, is explained; second, a three-dimensional intake model with integrated measurement equipment is presented and some important vocabulary is introduced; and third, the different conditions that were investigated during the measurement campaign are listed together with a general starting experiment time chart.

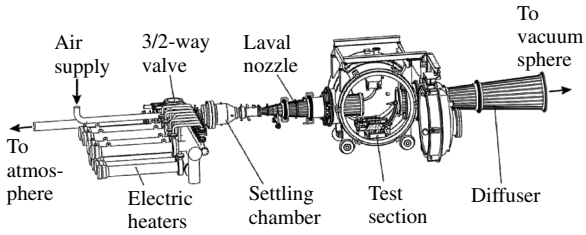

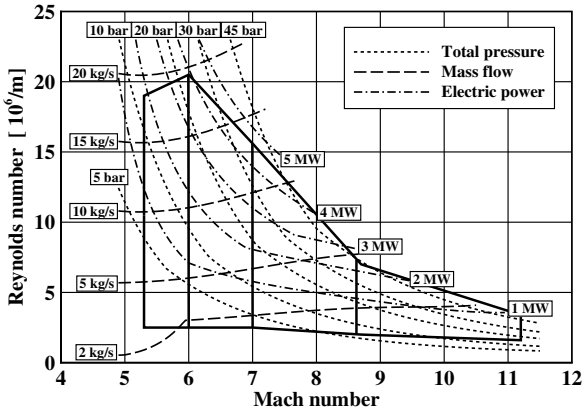

Fig. 2 Schematic setup of the H2K wind-tunnel (left) along with characteristic diagram (right).

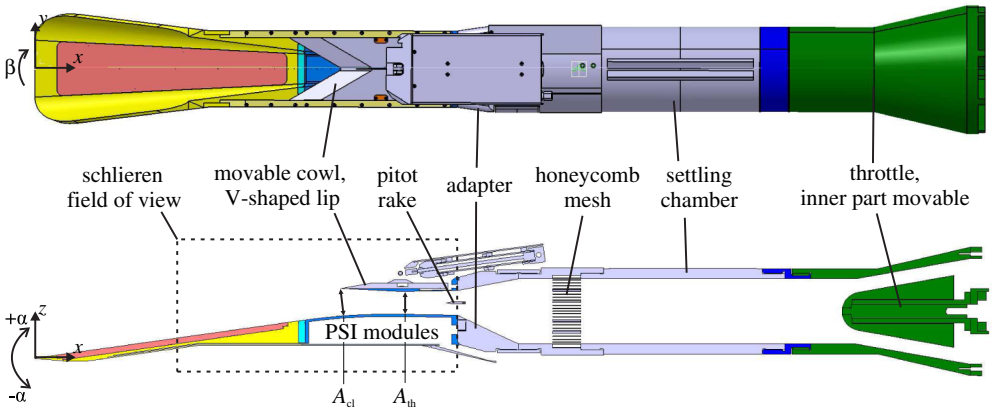

Fig. 3 Top and cross-sectional view of the three-dimensional intake.

A. Wind-Tunnel H2K

The experiments were performed in the blowdown wind tunnel H2K of the Supersonic and Hypersonic Technology Department at DLR, Cologne, Germany. A general sketch of the wind-tunnel setup along with a flow conditions diagram is shown in Fig. 2.

During operation, air is heated in the electric heater up to temperatures of approximately $T_{t,\infty} = 700$ K. During this period, the 3/2-way valve directs the airstream into the open atmosphere. Once the temperatures are reached, the valve is triggered and redirects the air through the settling chamber and Laval nozzle into the test section, where a model is located, before passing through the diffuser and into a vacuum sphere. There are five different Laval nozzles to create test Mach numbers of 5.3, 6, 7, 8.7, and 11.2, all having a circular cross-sectional exit area with a diameter of 600 mm. Depending on the desired conditions, test durations of about 35 s can be achieved.

B. Intake Model

The three-dimensional intake was designed with a computational-fluid-dynamics parameter study by Hohn and Gülhan [18] and Riehmer and Gülhan [19]. A top as well as cross-sectional view of the CAD model are displayed in Fig. 3. It was designed for Mach 8 flight at 30 km altitude, which corresponds to a freestream pressure, temperature, and unit Reynolds number of 1170 Pa, 226 K, and 2.95×10^6 m^{-1}, respectively. The dynamic pressure

$$q_\infty = \frac{1}{2}\rho_\infty v_\infty^2 \tag{5}$$

at the design point is approximately 0.53 bar.

The main ramp is inclined at an angle of 8 deg, whereas each side wall converges at a 7 deg angle. Along the centerline of the bottom and top walls, as well as in the axially movable cowl, there are static pressure sensors, and the pressure ducts run into the casing of the Pressure Systems, Inc. (PSI) modules. A pitot rake is positioned where the intake normally would end and the combustion chamber would start, which will be explained in more detail shortly. The uncertainty of the PSI modules was ±0.1% of the full scale, which corresponded to ±100 Pa. For our experiments, an adapter was attached to the intake, and the captured airflow went through a honeycomb mesh and a settling chamber before exiting through an axisymmetric throttle [20]. With this throttle, a backpressure could be imposed on the intake, and the captured mass flow could be measured. Furthermore, a schlieren imaging system was installed [21], and the field of view captured mainly the shock structure of the main ramp and near the cowl closure position. The length from the intake leading edge to the position of the pitot rake is 720 mm, and the intake throat is located at 650 mm. Because of the movable cowl, the internal contraction ratio CR_i could be varied from 1.28 to 2.56.

In addition to the *V*-shaped lip, displayed in Fig. 3, a straight lip was manufactured and a general sketch of the two different lip configurations is displayed in Fig. 4. The lip position, x_{lip}, was defined as the location where the cowl closed and the internal part of the intake started. The lip position was measured with a potentiometer and the uncertainty was ±0.25 mm. The relation between x_{lip} and the internal contraction ratio CR_i is given in Fig. 5, and it is noted that a change in the lip position of 1 mm corresponded to a change in internal contraction of ≈0.01.

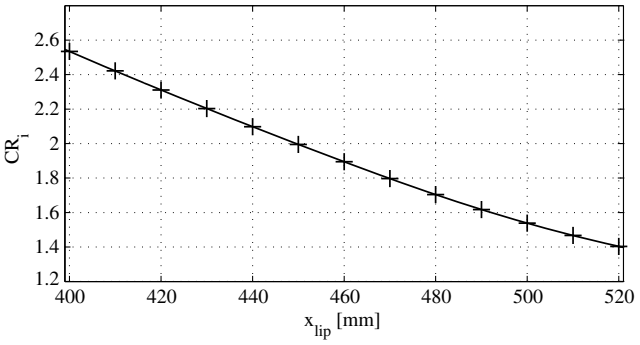

Fig. 5 Internal contraction ratio CR_i plotted vs lip position x_{lip}.

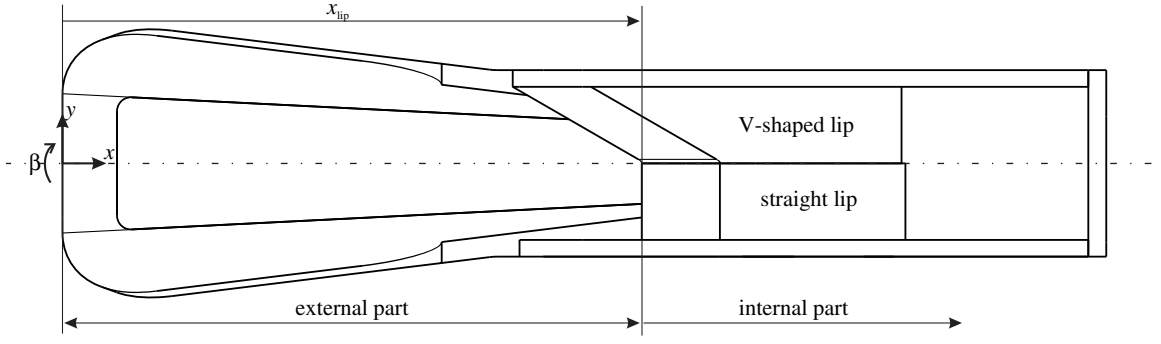

Fig. 4 Sketch of intake with *V*-shaped (shown top) and straight (shown bottom) cowl lip.

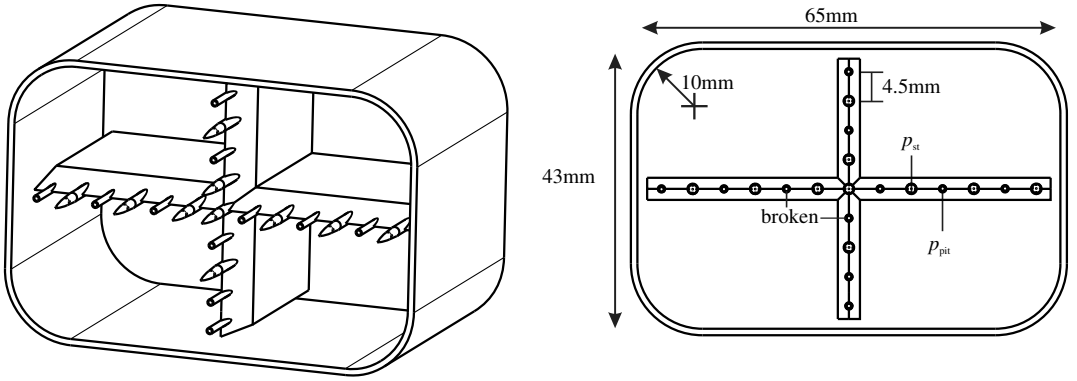

Fig. 6 Pressure rake, with pitot and static [22] pressure tubes.

The dimensions of the intake exit area were 43×65 mm^2 with radiused corners (Fig. 6). The pressure probes consisted of alternately distributed pitot as well as static pressure ports [22], and therefore static and pitot pressures were measured. Pinckney investigated the pressure probes up to 12 deg angle of attack [22]. Although the maximum deviation was ≈10%, no certain trend could be determined. In our analysis, we calibrated the probes at zero angle of attack in a separate wind tunnel for Mach numbers ranging from 1.5 to 4.5. The data of two pressure probes were corrupt during the experimental campaign and therefore were interpolated from the neighboring values. To determine a pitot pressure at the location of a static pressure port and vice versa, the respective data were interpolated from their neighboring values. From these data, the Mach number across the intake exit height and width was calculated with the following equations; to determine whether there is super- or subsonic flow at the intake exit, the ratio of pitot to static pressure had to be checked, and if $p_{\text{pit}}/p_{\text{st}} > 1.893$, then the flow was supersonic. For supersonic flow, the relation is given via

$$\frac{p_{\text{pit}}}{p_{\text{st}}} = \left[\frac{(\gamma+1)^2 M^2}{4\gamma M^2 - 2(\gamma-1)}\right]^{\gamma/(\gamma-1)} \frac{1-\gamma+2\gamma M^2}{\gamma+1} \tag{6}$$

and the Mach number was calculated iteratively, for example with Newton's method [23]. For subsonic flow, the following equation was directly applied to calculate the Mach number:

$$M^2 = \frac{2}{\gamma-1}\left[\left(\frac{p_{\text{pit}}}{p_{\text{st}}}\right)^{(\gamma-1)/\gamma} - 1\right] \tag{7}$$

For further information on calculating the Mach number from pitot pressure, see for example the introductory textbook by Anderson [5]. To obtain one-dimensional intake exit data for a sample variable ϕ, the average over all pressure probes was calculated:

$$\bar{\phi} = \frac{1}{n}\sum_{j=1}^{n=21} \phi_j \tag{8}$$

To calculate an averaged Mach number or total pressure, the values were initially calculated at each location, and subsequently Eq. (8) was applied.

C. Experimental Campaign

An overview of the different wind-tunnel conditions that were investigated is given in Table 1. Two different Mach numbers were examined, and the respective Reynolds numbers were adjusted to altitudes that matched a trajectory with constant dynamic pressure $q_\infty = 0.53$ bar. The wall temperature of the model was assumed to be constant ($T_w = 300$ K), and part of the campaign was to vary the total temperature of the freestream. Furthermore, the V-shaped (V) and straight (S) lip were investigated to evaluate differences in the starting process.

The influence of pitch α and yaw angle β on intake starting also was investigated. Both angles were varied separately, but also simultaneously, as indicated in Table 2. For reasons of symmetry, β was varied only in the positive direction.

In Fig. 7, a sample time chart of a general starting experiment is plotted. Note that the only dependent variable shown quantitatively is x_{lip} (solid line), whereas the other variables are displayed for qualitative reasons only (broken lines). Initially, the cowl is at the most upstream position, and the intake is unstarted, which is indicated by the low total pressure ratio (short dashed line), defined as

$$\Pi_{\text{tot}} = \frac{p_{t,\text{exit}}}{p_{t,\infty}} \tag{9}$$

which is a measure of intake compression efficiency. The static pressure ratio, which will emerge in Sec. III, is analogously defined as:

$$\Pi_{\text{st}} = \frac{p_{\text{st,exit}}}{p_{\text{st},\infty}} \tag{10}$$

After the tunnel was started, the freestream static pressure adjusted within a couple of seconds. For the temperature measurement, a type K thermocouple (class 1) was used. The thermocouple was placed in the airstream in front of the Laval nozzle and mounted in a robust housing to withstand the aerodynamic loads. Because of this robust housing and the relatively low-density airstream, the measured total temperature only slowly approached steady state. Approximately 3 s after the tunnel was started, the cowl was moved backward with a constant velocity, reducing the internal contraction ratio accordingly. In a previous study, a lower velocity did not have an effect on the

Table 1 Overview of different test conditions, for constant wall temperature $T_w = 300$ K

M_∞	$T_{t,\infty}/T_w$	Re (×10^6), m^{-1}	Lip geometry	Respective altitude, km
7 ± 0.05	2.33 ± 0.05	3.39	V[a]	28.2
7 ± 0.05	2.00 ± 0.05	3.39	V[a]	28.2
7 ± 0.05	1.67 ± 0.05	3.39	V[a]	28.2
7 ± 0.05	2.33 ± 0.05	3.39	S[b]	28.2
6 ± 0.05	2.33 ± 0.05	4.00	V[a]	26.2

[a]V-shaped lip.
[b]Straight lip.

Table 2 Overview of angle-of-attack configurations that have been investigated

	α, deg				
β, deg	−4	−2	0	2	4
0	×	×	×	×	×
2		×	×	×	
4			×		

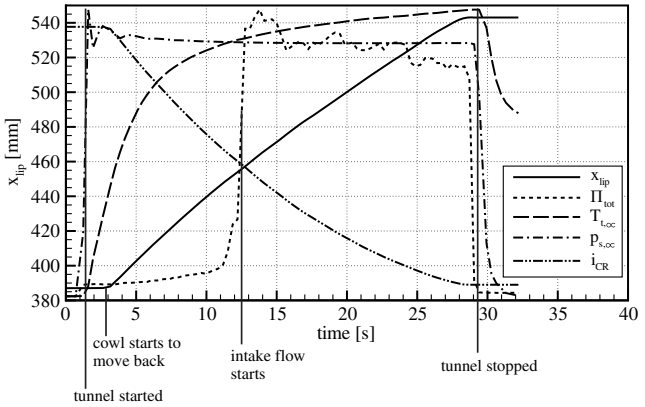

Fig. 7 Time chart of general starting experiment.

starting behavior [18]. The time scale of the flow is on the order of 10^{-2}–10^{-4} s [24], whereas in the present paper, the internal contraction ratio is given with an accuracy of 0.01, which approximately corresponded to a change in x_{lip} of about 1 mm. The time it took the cowl to travel 1 mm was 0.15 s, and therefore the time scale of the flow was assumed to be at least one order of magnitude lower than the time scale of the cowl movement. Started intake flow was indicated by a sharp increase in total pressure measured at the rake, which in Fig. 7 occurs at approximately 12.5 s. Finally, after 29 s, the cowl reached the most downstream position and the tunnel flow was stopped.

III. Results

Here, we will present the influence of Mach number, cowl geometry, angle of attack, and total temperature on intake starting. For better understanding, the principle display of the figures will be identical: The independent variable is internal contraction ratio CR_i, and it is plotted as the horizontal axis. In the top portion of Figs. 8–12, the total pressure ratio Π_{tot} is plotted; in the middle portion, the static pressure ratio Π_{st} is plotted; and in the bottom portion, the intake exit Mach number M_{exit} is plotted. These variables will be referred to as performance parameters in the subsequent sections. As seen in Fig. 7, the internal contraction ratio is reduced with time, and therefore the figures need to be read from right to left. Furthermore, the configuration with the *V*-shaped lip at Mach 7 and no angle of attack will be considered as a reference case and is plotted twice to illustrate run-to-run variations during two experiments. Because of time constraints during the measurement campaign, experiments were usually performed only once, and therefore no data to investigate the run-to-run variations for the other configurations are available. However, the general procedure shown in Fig. 7 was satisfied during all starting experiments.

A. Cowl Shape

The influence of the lip geometry on intake starting is first discussed for a freestream Mach number of 7, and results are plotted in Fig. 8 (solid and long dashed lines). For high internal contraction ratios ($\text{CR}_i > 2.3$), the intake flow is subsonic, and the total pressure ratio is at an insufficient level (less than 0.05). As the internal contraction ratio reduces, supersonic intake flow is established. For the straight lip, the intake starts earlier (at $\text{CR}_i = 2.12$) than for the *V*-shaped lip (at $\text{CR}_i = 1.92$). Shortly before both configurations start, a plateau region is formed, where the flow through the intake is already supersonic ($M_{\text{exit}} \approx 2$) but where the total pressure ratio is still at a poor level ($\Pi_{\text{tot}} \approx 0.12$). The plateau region is more distinct for the straight lip than for the *V*-shaped lip but is visible for both cases. For low internal contraction ratios ($\text{CR}_i < 1.9$), the intake flow is fully established, and the Mach number and static and total pressure ratios at the exit are approximately: $M_{\text{exit}} \approx 3$, $\Pi_{\text{st}} \approx 33$, and $\Pi_{\text{tot}} \approx 0.4$, respectively.

At the same x_{lip} position, the *V*-shaped cowl captures more airflow compared to the simple straight-lip geometry. Therefore, the effect of overboard spillage, as explained in [10], becomes more distinct for the straight-lip configuration, and the starting position moves to higher internal contraction ratios.

In Fig. 1, the starting internal contraction ratios for the different cowl geometries are plotted. To calculate the Mach numbers at the cowl closure positions, Reynolds-averaged Navier–Stokes simulations were performed with the finite-volume DLR-TAU solver [25]. At the cowl closure positions, planes were extracted, and the mass-averaged Mach numbers were calculated with a self-written Matlab (R2012a) routine. For both configurations, the internal contraction ratios fall within the region where the intake would not be self-starting due to the Kantrowitz theory. However, both configurations are very close to the linear fit by Sun and Zhang [11] and deviate slightly from the quadratic fit by Smart [12].

To further illustrate the flowfield during the starting process, in Fig. 9, schlieren images are plotted for the started and the unstarted case as well as for the plateau region. In the unstarted condition, there is a strong shock behind which the flow is subsonic, and a large amount of spillage is present. For the started condition, sharp shock structures establish and the airflow is entirely supersonic. In between,

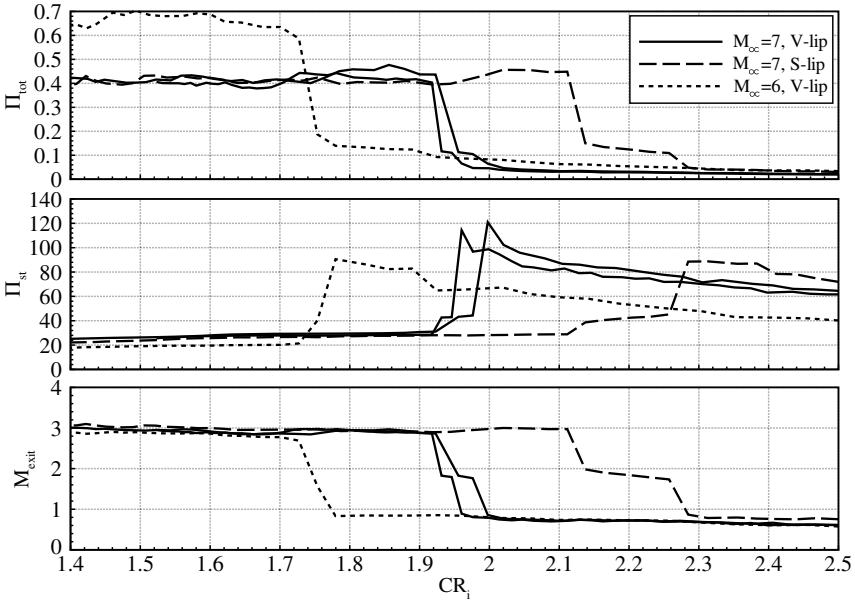

Fig. 8 Starting behavior for different freestream Mach numbers and different cowl geometries.

Table 3 Captured mass flow for different configurations

	$M_\infty = 7$, V-lip	$M_\infty = 7$, S-lip	$M_\infty = 6$, V-lip
$\dot{m}_\infty$, kg/s	0.301	0.301	0.481
$\dot{m}_{\text{intake}}/\dot{m}_\infty$	0.877	0.867	0.686

the strong shock is still visible, which explains the low total pressure recovery (Fig. 8, top). However, behind the strong shock, there are oblique shock structures, which suggest that the flow is at least partially supersonic. In numerical simulations, we were able to reproduce the started condition only, and therefore we were not able to draw any further conclusions regarding the different staring modes.

Finally, in Table 3, the different mass capture ratios, $\dot{m}_{\text{intake}}/\dot{m}_\infty$, which we measured with the attached throttle, are displayed. It is noted that, even though the straight-lip configuration is self-starting at a larger internal contraction ratio, its capture ratio is slightly lower (1%) than for the V-lip configuration.

B. Mach Number

Results for the Mach-number variation are plotted along with the lip geometry results in Fig. 8. For the lower test Mach number of 6, intake starting is delayed to a lower internal contraction ratio ($\text{CR}_i \approx 1.72$). Although the exit Mach number for started intake flow remains approximately constant, the static pressure ratio drops to $\Pi_{\text{st}} \approx 22$ for the lower freestream Mach number. However, the total pressure ratio rises to $\Pi_{\text{tot}} \approx 0.60$. Observing Fig. 8, it is unclear if a plateau region exists for the lower Mach number. Because to this point no other data are available, no further comment on the plateau for the Mach 6 case is made.

When looking at the Kantrowitz diagram (Fig. 1), the internal contraction ratio for starting is again within the region where intake starting should not occur according to the Kantrowitz theory but was close to the linear prediction [11]. Furthermore, the effect of delayed intake starting due to lower freestream Mach number can be explained: A reduced freestream Mach number leads to a reduced Mach number at the cowl closure position as well. Moving to the left in the Kantrowitz diagram leads to a decreased internal contraction ratio for intake starting. Please note that, in Fig. 1, the reciprocal value of CR_i is given and that the Mach numbers at the cowl closure position were again obtained from numerical simulations.

In search of the intake maximum operating contraction ratio, for the V-lip configuration, the intake cowl was moved upstream from a position where the intake flow was started to the maximum forward position. For the maximum internal contraction ratio of 2.56, the intake flow was still started for both Mach numbers investigated. With the current model, we were therefore unable to determine the maximum allowable internal contraction ratio, following proper intake starting.

C. Angle of Attack

The angle-of-attack influence on intake starting was investigated per the conditions in Table 2. Display of the data follows the layout in the previous subsection, and results for pitch-angle variation are plotted in Fig. 10. Note that a positive α is equal to lifting the intake nose and is therefore equal to a lower deflection caused by the main ramp, and vice versa (see also Fig. 3 for the angle description).

A positive pitch angle leads to earlier intake starting, whereas a negative pitch angle delays intake starting. When going to pitch angles as high as ± 4 deg, the change in CR_i can reach as high as 0.3. The performance parameters for started intake flow are influenced as follows: With an increased α, the static pressure ratio drops, whereas the exit Mach number and total pressure ratio increase, and vice versa. Except for the $\alpha = -4$ deg case, the plateau region with supersonic flow in the intake is present for all configurations.

To explain the influence of α, one can imagine what happens to the flow when the intake is pitched. As stated earlier, by lifting the intake

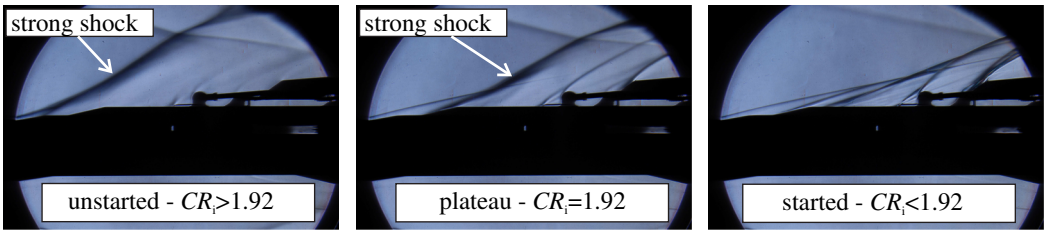

Fig. 9 Schlieren images of unstarted, started, and plateau case for $M_\infty = 7$ and the V-shaped lip configuration.

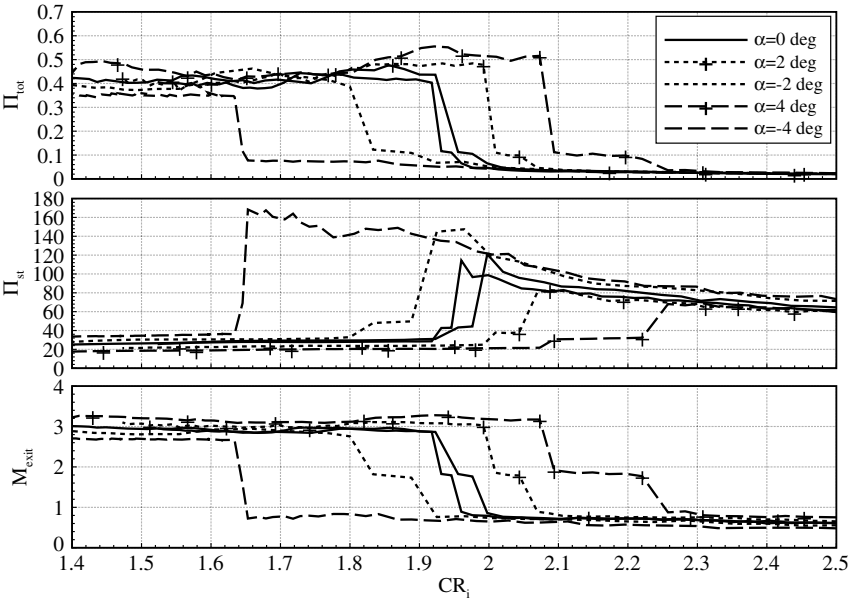

Fig. 10 Influence of pitch angle α variation on starting behavior of intake; yaw angle was kept zero.

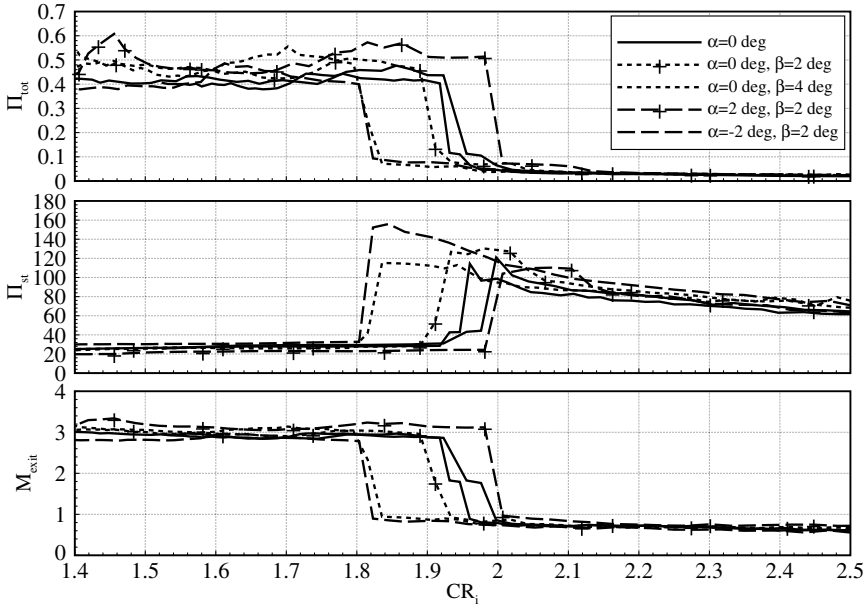

Fig. 11 Influence of yaw angle β and of simultaneous pitch and yaw angle on intake starting for *V*-shaped lip at Mach 7.

nose, the deflection caused by the main ramp decreases, and therefore the leading-edge shock loses strength. This then leads to a higher Mach number behind the leading-edge shock and, in the first approximation, to a higher Mach number at the cowl closure position. Analogous to the previous section, intake starting is enhanced by this higher Mach number.

Furthermore, the influence of a yaw-angle variation on the intake starting behavior was investigated, and results are plotted in Fig. 11 as dotted lines. A moderate yaw angle of $\beta \approx 2$ deg only marginally delayed intake starting, whereas further increasing β to 4 deg delayed intake starting to $\mathrm{CR}_i \approx 1.8$. Thus, for the angles considered, there is a maximum change in internal contraction ratio of about 0.1. For symmetry reasons, the yaw angle was varied only in one direction.

When increasing the yaw angle, the deflection angle at the sidewalls that the flow sees behaves twofold: the leading-edge shock on one side wall becomes stronger, whereas the shock strength on the other side wall decreases. The influence of yaw angle is therefore less than the influence of pitch angle.

In a possible flight experiment with a sounding rocket, during the ascent, the experiment would first leave the atmosphere and then reenter with hypersonic velocities. During reentry, the targets usually contain some form of tumbling motion [26]. To reproduce the intake starting behavior during this tumbling motion or during a vehicle maneuver in general, both α and β were varied simultaneously, and results are plotted along with the yaw-angle variation in Fig. 11. One can see that the effects of improved starting due to a positive pitch angle, and the effect of delayed intake starting due to yaw angle, are to an extent superposable. One can therefore conclude that, during a possible tumbling motion or maneuver of the scramjet engine in a flight experiment, there are going to be regions where intake starting is enhanced (large α and β near zero) and regions with delayed intake starting, when compared to the zero angle of attack condition.

D. Total Temperature

The $T_{t,\infty}/T_w$ (flow total temperature to wall temperature) ratio was varied from 1.66 to 2.33, which approximately corresponds to wall temperatures of 1000–1400 K for a real flight condition at Mach 7. The influence of the temperature variation on intake starting is plotted in Fig. 12. A higher temperature ratio favors intake starting to higher internal contraction ratios. In other words, for colder walls, the intake

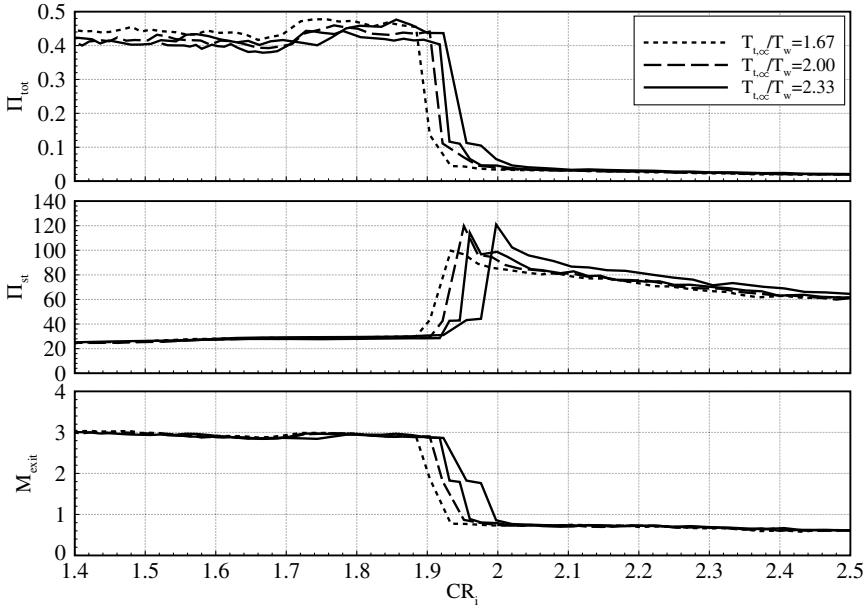

Fig. 12 Starting behavior for various total temperature ratios for *V*-shaped lip at Mach 7.

shows improved starting characteristics. For lower temperature ratios, the plateau region with supersonic flow at the intake exit disappears. However, the maximum change in CR_i is only around 0.04, and therefore the overall influence of total temperature to wall temperature ratio on intake starting is weak, at least in the temperature ranges considered.

IV. Conclusions

In the current paper, experimentally observed insights into the starting behavior of a three-dimensional scramjet intake are presented, with variable internal contraction at the two Mach numbers $M_\infty = 6, 7$. Experiments were performed in the H2K blowdown wind tunnel. The four main research topics included the influence of 1) cowl geometry, 2) Mach number, 3) angle of attack, and 4) freestream total temperature to wall temperature ratio on intake starting. The airflow through the intake duct was analyzed at the intake exit area with a rake containing static as well as pitot pressure ports, and the performance parameters of exit Mach number and total and static pressure ratio were calculated from the measured data. The following main conclusions can be drawn from the presented results:

1) For configurations with no angle of attack, the internal contraction ratios for intake starting were found to be higher than the values predicted by the Kantrowitz theory. Therefore, the Kantrowitz line should be considered as a conservative measure, especially for high-speed, three-dimensional intakes.

2) Once the intake was started, increasing the internal contraction ratio to values as high as 2.56 did not cause an intake unstart for either Mach number investigated.

3) The straight-cowl geometry significantly improved the starting behavior from an internal contraction ratio of 1.92 for the *V*-shaped lip to 2.12. This phenomenon is mainly caused by the increase in overboard spillage for the straight-cowl geometry. However, the mass capture ratio for the *V*-lip configuration was approximately 1% larger than for the straight-lip configuration.

4) With decreasing freestream Mach number, intake starting was reduced to lower internal contraction ratios, which correlates with Kantrowitz theory. However, the internal contraction ratio was still within the region where intake starting is not guaranteed to occur according to this one-dimensional flow theory.

5) Angle-of-attack effects were twofold: For positive pitch angles, intake starting was enhanced, whereas for negative pitch angles and increasing yaw angles, intake starting was delayed. Overall, the pitch angle influence was stronger.

6) Finally, varying the freestream total to wall temperature ratio from 1.67 to 2.33 had only a minor effect on the starting behavior.

Acknowledgments

The authors would like to thank the German Research Foundation for the support of the Scramjet Research Training Group 1095. Furthermore, we would like to thank Michael Kosbow and Marco Schmors, both from the Supersonic and Hypersonic Technology Department, for operation of the H2K wind tunnel and technical support.

References

[1] Heiser, W. H., and Pratt, D. T., *Hypersonic Airbreathing Propulsion*, AIAA Education Series, AIAA, Washington, D.C., 1994, pp. 22–26, Chap. 1.

[2] Hermann, R., *Supersonic Inlet Diffusers and Introduction to Internal Aerodynamics*, Minneapolis-Honeywell Regulator Co., Minneapolis, MN, 1956, pp. 33–53, Chap. 2.

[3] Oswatitsch, K., "Pressure Recovery for Missiles with Reaction Propulsion at High Supersonic Speeds," NACA TM-1140, 1944.

[4] Kantrowitz, A., and Donaldson, C., "Preliminary Investigation of Supersonic Diffusers," NACA ACR-L5D20, 1945.

[5] Anderson, J. D. J., *Fundamentals of Aerodynamics*, 4th ed., McGraw–Hill, New York, 2007, pp. 548–552, Chap. 8.

[6] Goldberg, T. J., and Hefner, J. N., "Starting Phenomena for Hypersonic Inlets with Thick Turbulent Boundary Layers at Mach 6," NASA TN-6280, 1971.

[7] Ogawa, H., Grainger, A. L., and Boyce, R. R., "Inlet Starting of High-Contraction Axisymmetric Scramjets," *Journal of Propulsion and Power*, Vol. 26, No. 6, Nov. 2010, pp. 1247–1258. doi:10.2514/1.48284

[8] Wie, D. M. V., Kwok, F. T., and Walsh, R. F., "Starting Characteristics of Supersonic Inlets," *32nd AIAA/ASME/SAE/ASEE Joint Propulsion Conference and Exhibit*, AIAA Paper 1996-2914, July 1996.

[9] Mölder, S., Timofeev, E. V., and Tahir, R. B., "Flow Starting in High Compression Hypersonic Air Inlets by Mass Spillage," *40th AIAA/ASME/SAE/ASEE Joint Propulsion Conference and Exhibit*, AIAA Paper 2004-4103, July 2004.

[10] Veillard, X., Tahir, R., Timofeev, E., and Mölder, S., "Limiting Contractions for Starting Simple Ramp-Type Scramjet Intakes with Overboard Spillage," *Journal of Propulsion and Power*, Vol. 24, No. 5, 2008, pp. 1042–1049. doi:10.2514/1.34547

[11] Sun, B., and Zhang, K.-Y., "Empirical Equation for Self-Starting Limit of Supersonic Inlets," *Journal of Propulsion and Power*, Vol. 26, No. 4, 2010, pp. 874–875. doi:10.2514/1.46798

[12] Smart, M. K., "How Much Compression Should a Scramjet Inlet Do?" *AIAA Journal*, Vol. 50, No. 3, 2012, pp. 610–619. doi:10.2514/1.J051281

[13] Jacobsen, L. S., Tam, C.-J., Behdadnia, R., and Billig, F. S., "Starting and Operation of a Streamline-Traced Busemann Inlet at Mach 4," *42nd AIAA/ASME/SAE/ASEE Joint Propulsion Conference and Exhibit*, AIAA Paper 2006-4508, July 2006.

[14] Smart, M. K., "Design of Three-Dimensional Hypersonic Inlets with Rectangular-to-Elliptical Shape Transition," *Journal of Propulsion and Power*, Vol. 15, No. 3, May 1999, pp. 408–416. doi:10.2514/2.5459

[15] Billig, F. S., and Kothari, A. P., "Streamline Tracing: Technique for Designing Hypersonic Vehicles," *Journal of Propulsion and Power*, Vol. 16, No. 3, 2000, pp. 465–471. doi:10.2514/2.5591

[16] Mölder, S., and Szpiro, E. J., "Busemann Inlet for Hypersonic Speeds," *AIAA Journal*, Vol. 3, No. 8, 1966, pp. 1303–1304. doi:10.2514/3.28649

[17] Timofeev, E. V., Tahir, R. B., and Mölder, S., "On Recent Developments Related to Flow Starting in Hypersonic Air Intakes," *15th AIAA International Space Planes and Hypersonic Systems and Technologies Conference*, AIAA Paper 2008-2512, May 2008.

[18] Hohn, O. M., and Gülhan, A., "Analysis of a Three-Dimensional, High Pressure Ratio Scramjet Inlet with Variable Internal Contraction," *18th AIAA/3AF International Space Planes and Hypersonics Systems and Technologies Conference*, AIAA Paper 2012-5975, Sept. 2012.

[19] Riehmer, J. C., and Gülhan, A., "Simulation of Combustion by Cold Air Injection in a Generic Scramjet Model in the H2K Blow Down Facility," *Proceedings of the 5th European Conference for Aeronautics and Space Sciences*, EUCASS Association, Les Ulis Cedex, France, July 2013, http://www.eucass-proceedings.eu/.

[20] Triesch, K., and Krohn, E.-O., "Verwendung von Kegeldüsen zur Drosselung und Durchsatzmessung bei Überschalleinläufen," DLR, German Aerospace Center, TR IB-39113-83-A-04, Cologne, Germany, 1984.

[21] Tropea, C., Yarin, A. L., and Foss, J. F., *Handbook of Experimental Fluid Mechanics*, Springer, Berlin, 2007, pp. 476–478, Chap. 6.

[22] Pinckney, S. Z., "An Improved Static Probe Design," *AIAA Journal*, Vol. 12, No. 4, 1973, pp. 562–564. doi:10.2514/3.49289

[23] Arens, T., Hettlich, F., Karpfinger, C., Kockelkorn, U., Lichtenegger, K., and Stachel, H., *Mathematik*, Spektrum Akademischer, Heidelberg, Germany, 2008, p. 292, Chap. 10.

[24] Segal, C., *The Scramjet Engine: Processes and Characteristics*, Cambridge Aerospace Series, Cambridge Univ. Press, New York, 2009, pp. 128–129, Chap. 6.

[25] Mack, A., and Hannemann, V., "Validation of the Unstructured DLR-TAU-Code for Hypersonic Flows," *32nd AIAA Fluid Dynamics Conference and Exhibit*, AIAA Paper 2002-3111, June 2002.

[26] Gülhan, A., Siebe, F., Thiele, T., Neeb, D., Turner, J., and Ettl, J., "Sharp Edge Flight Experiment-II Instrumentation Challenges and Selected Flight Data," *Journal of Spacecraft and Rockets*, Vol. 51, No. 1, Jan. 2014, pp. 175–186. doi:10.2514/1.A32572

R. Lucht
Associate Editor